GSA DATA REPOSITORY 2012065

Lachniet et al., A 2400-yr Mesoamerican rainfall reconstruction links climate and cultural change

Methods and Results

Stalagmite JX-6 was sectioned in half and subsampled for stable ($\delta^{18}O$ and $\delta^{13}C$) isotopes by micromilling at 0.25 mm intervals (sub-annual resolution) over the upper 80 mm of calcite growth, and 1-mm intervals (ca. 3-yr resolution) between 81 and 990 mm depth, yielding a total of 1230 samples. Samples were analyzed at the Las Vegas Isotope Science Lab (LVIS), by phosphoric acid reaction at 70ºC. Water $\delta^{18}O$ and δD were determined on a TC/EA device. Values are reported in ‰ relative to the VPDB and VSMOW standards, with precisions better than 0.08‰ and 0.15‰ $\delta^{18}O$ for carbonates and waters, respectively, and ± 0.08‰ $\delta^{13}C$. Water sample values were calibrated with internal standards on a scale where values of SLAP are -55.5 and -428‰ for $\delta^{18}O$ and δD, respectively.

Stalagmite $\delta^{18}O$ values range between -6.8 and -9.4‰ VPDB, and mostly vary by ~1.5‰. Variations in $\delta^{18}O$ are characterized by a lag-1 autocorrelation coefficient of r = 0.76, suggesting a non-noisy signal with a large signal to noise ratio. The 1.5‰ variability is significantly larger than the 0.1‰ analytical uncertainty for $\delta^{18}O$ analyses. Additional evidence that signal represents a true climate signal is the correlation between JX-6 $\delta^{18}O$ and rainfall amount in Mexico City.

To determine the $\delta^{18}O$ value typical of the cave region, we collected 43 surface water samples in the Sierra Madre del Sur and Balsas River basin, near Juxtlahuaca Cave, to constrain modern $\delta^{18}O$ values. Two visits to Juxtlahuaca Cave occurred during the dry season when drips were very slow, so drip samples could not be collected. The mean $\delta^{18}O$ value of the surface water is -8.3 ± 1.1 ‰. The average $\delta^{18}O$ values of a cave pool ("Fuente Encantada") is -7.6‰, and that of the Rio Blanco adjacent to the cave site is -8.5‰, both of which are likely within the range for drip and rainfall values in Juxtlahuaca Cave.

U-series isotope measurements were done at the Radiogenic Isotope Laboratory, University of New Mexico. Subsample powders (50-200 mg) were dissolved in nitric acid and spiked with a mixed ^{229}Th-^{233}U-^{236}U spike. The U and Th isotope analysis was done on a Thermo Neptune multi-collector inductively coupled plasma mass spectrometer (MC ICP-MS)(Asmerom et al., 2006). U isotope values are reported as ‰ variations in the $^{234}U/^{238}U$ from secular equilibrium [$\delta^{234}U = [[^{234}U/^{238}U_{sample}/\ ^{234}U/^{238}U_{secular\ equilibrium}]-1] \times 10^3$, where $^{234}U/^{238}U_{secular\ equilibrium} = \lambda_{238}/\lambda_{234}$, $\lambda_{230} = 9.1577 \times 10^{-6}\ y^{-1}$, $\lambda_{234} = 2.8263 \times 10^{-6}\ y^{-1}$, $\lambda_{238} = 1.55125 \times 10^{-10}\ y^{-1}$ (Cheng et al., 2000). Analytical uncertainties are 2-σ of the mean; age uncertainties include analytical errors and uncertainties in the initial $^{230}Th/^{232}Th$ ratios, which is equal to 4.4 ppm (assuming a bulk earth $^{232}Th/^{238}U$ value of 3.8). Uncertainties in the initial $^{230}Th/^{232}Th$ ratios and Th and U blanks (5 and 10 picograms for the procedure) did not make difference in the age of the samples. Stalagmite growth rates were determined by linear interpolation between the U-series ages. The U-series data and ages are reported in Table 1.

For the spectral analysis we used REDFIT (Schulz and Mudelsee, 2002), which is optimized for unevenly-spaced climate data. Spectral variability is present in the ~4-10 yr bands for the raw $\delta^{18}O$ data. The ~4-yr periods arise from the high-resolution (0.25 mm) subsampling for the most recent centuries.

Study Area and Modern Climate

Figures DR1 and DR5 show the study area and sites mentioned in the text and mean annual precipitation (Sáenz-Romero et al., 2010). The climate of southwestern and central Mexico is dominated by summer convection associated with the southern branch of the North American Monsoon System (Adams and Comrie, 1997; Barlow et al., 1998; Higgins et al., 1999) (alternatively known as the Mexican Monsoon (Douglas et al., 1993; Stensrud et al., 1995)). The NAMS begins with convective rainfall over southwestern Mexico in late May and the center of convective activity shifts northward throughout the late summer/early fall seasons (Amador et al., 2006; Higgins et al., 1999; Stensrud et al., 1995). Monsoonal circulation results in strong convection (Cavazos and Hastenrath, 1990; Cortez-Vazquez, 1999) and upward vertical velocity (Barlow et al., 1998; Schmitz and Mullen, 1996) when the easterly and southerly winds converge over southern Mexico. Precipitation during the summer wet season is linked to moisture transport from both oceans (Barlow et al., 1998). Onshore winds due to diurnal heating also promote afternoon convection (Curtis, 2004; Mosiño-Alemán and García, 1974; Stensrud et al., 1995) along the Pacific coastline and Sierra Madre del Sur. During boreal winter, cold high-latitude air masses known as *nortes* (Chelton et al., 2000) may reach Central America and parts of east coastal Mexico (Mosiño-Alemán and García, 1974) but our study area is effectively blocked from their direct influence by the Mexican altiplano (Lauer, 1973; Mosiño-Alemán and García, 1974; Schultz et al., 1997). Thus, rainfall intensity over our study and in the Basin of Mexico is dominated by convection processes associated with monsoon rainfall.

Rainfall at the study area, based on climate normals from the town of Colotlipa 3 km south of Juxtlahuaca Cave at an altitude of 840 m, averages 1163 mm/yr, most of which falls during the June to November wet season (Servicio_Meteorológico_Nacional, 2008). Annual evaporation is 2081 mm, indicating an annual moisture deficit, and mean annual temperature is 24.6°C. The seasonal range in temperature is <4ºC, which is typical of tropical latitudes.

Influence of ENSO on Monsoon Rainfall

Several studies have confirmed that ENSO has a strong effect on rainfall amount in the monsoon regions of Mexico (Higgins et al., 1999; Jauregui, 1995; Mosiño and Morales, 1988). Drought conditions are statistically linked with warm El Niño events at the 0.001 level (Jauregui, 1995). Drier conditions during El Niño are associated with fewer tropical disturbances reaching Mexico from both the Gulf of Mexico and Pacific Ocean. In tropical Mexico, El Niño droughts result in reduced river flows, reservoir levels and water availability, increased forest fires, and agricultural disruption (Magaña, 2004; Magaña et al., 2003). Negative precipitation anomalies are associated with El Niño warm events over the northern tropical Americas, related to a shift in the Walker circulation, enhanced subsidence, and a southward shift of the eastern tropical Pacific ITCZ (Dai and Wigley, 2000; Rogers, 1988). ENSO is also the dominant control on rainfall variability in southwestern Mexico (Figure DR6) (Cavazos and Hastenrath, 1990; Higgins et al., 1999; Jauregui, 1995; Wang and Fiedler, 2006). The correlation (and precipitation anomalies) for wet and dry ENSO events are $r = 0.67$ (+10.6%) and $r = 0.71$ (-14.6%), respectively (Higgins et al., 1999). The El Niño rainfall decrease is also related to a weaker land-sea temperature contrast and a weaker monsoon (Higgins et al., 1999). A further possible control on ENSO rainfall anomalies is the number of landfalling eastern Pacific tropical storms, which decrease during El Niño years (Jauregui, 1995). In contrast to El Niño, rainier conditions are associated with cool La Niña events (Higgins et al., 1999). A 450-year record of historical droughts and famines from 1450 to 1900 A.D. in central Mexico showed a correspondence between drought and strong El Niño events (Mendoza et al., 2005). Analysis of rainfall data in southwestern and central Mexico show significant correlations to sea surface temperature in the tropical Pacific Ocean (Liebmann et al., 2008), demonstrate the effect of ENSO on controlling regional rainfall amount. The concordance of results showing modern and past El Niño drought implicates a dominant control of tropical Pacific ocean-atmosphere processes on summer rainfall in southwestern Mexico.

δ^{18}O/Climate Calibration

To determine the relationship between JX-6 δ^{18}O values and rainfall amount in the Basin of Mexico (Tacubaya Station), we regressed δ^{18}O values against rainfall for the period of 1880-2010 at various leads and lags. We first completed this correlation for the 1-yr interpolated δ^{18}O data and wet season (May through October) rainfall at the Tacubaya station, which is located on the former westernmost edge of Lake Texcoco 700 m south of Chapultepec Park (a source of spring discharge delivered to Aztec Tenochtitlán). Second, we repeated this calibration for δ^{18}O and rainfall data that was smoothed by a five-year running average (1882-2008 interval), to take account 1) the likely smoothing of the δ^{18}O signal during transit through the ~160-m thick epikarst overlying the cave, and 2) to emphasize the multi-annual rainfall variability that is most likely to be robustly captured in our stalagmite reconstruction. Third, we repeated the calibration for the time interval between 1882 to 1988 in order to remove those Tacubaya climate data that are likely to contain an anthropogenic influence (Juaregui, 1990/1991), and that clearly plot off the regression line determined for our 5-yr smoothed (1882-2008) calibration. For all correlations, we constructed lag correlograms for the JX-6 δ^{18}O time series between -25 yr (JX-6 lagging rainfall) and +25 yr (JX-6 leading rainfall), in order to empirically estimate drip transit and/or smoothing time for water transiting the cave epikarst. The start dates for the lagged correlations were varied to account for the lag interval.

Although our third calibration is somewhat subjective because of the selective removal of the post-1988 data, we feel that it is warranted because of the clear anthropogenic influence on climate in Mexico City in recent decades. The Tacubaya climate station is now located in a highly urban environment, but when initiated was in a semi-rural location. The station is also located adjacent to a large forested urban park (Chapultepec Park) with known urban microclimates (Juaregui, 1990/1991). Such an influence is apparent in the Tacubaya temperature history which shows that recent temperatures have exceeded historical (1880-1950) variability in the 1970s, around the time that the JX-6 $\delta^{18}O$ data diverge from the rainfall trends at Tacubaya (text Figure 2).

The lag correlograms (Figure DR2**)** show that $\delta^{18}O$ is most strongly correlated to rainfall amount when JX-6 lags rainfall amount by 5 to 11 years, with the strongest correlation of the smoothed data at 9 years. Our rainfall reconstruction is insensitive to choice of calibration equation, resulting in mean rainfall differences of less than 3.2% for the 1-yr 1880-2010 and the 5-yr smoothed 1880-1988 calibrations, respectively. For comparison of the three calibrations described above, the reconstructed mean wet season rainfall for the Basin of Mexico are 709 ± 125, 705 ± 139, and 686 ± 125 mm, respectively. These values compare favorably with the measured Tacubaya wet season rainfall amounts of 684 ± 163 mm (1880-2010).

Our $\delta^{18}O$ data, and analysis of climate data for Mexico, indicate a return to dry conditions in the 1990s (Stahle et al., 2009), a trend that is not evident in the Tacubaya rainfall data. The Mexico City climate data may be compromised by urban effects (Juaregui, 1992). The anomalous $\delta^{18}O$/Tacubaya rainfall signal after ca. 1988 may also be a manifestation of anomalous atmospheric circulation in an anthropogenically-altered climate, as the last few decades show a clearly anomalous warming above historical levels.

Links Between Mexico City and Juxtlahuaca Cave Rainfall Data

To assess the degree of similarity of the rainfall records between our study area and Mexico City, we compared the Tacubaya rainfall time series to data from Colotlipa, near the study area, to compare the seasonal cycles, and to rainfall time series extracted from the NCEP reanalysis data (Kalnay et al., 1996). The NCEP reanalysis data are the best-available data to compare with the Tacubaya rainfall amount, because individual station data from Mexico are not easily accessible. The NCEP data extend to 1941, and are thus less useful for comparing longer-term precipitation trends. We extracted wet season (MJJASO) rainfall for three areas around the study area: 1) The Sierra Madre del Sur (precip_02), 2) the Sierra Madre del Sur to the Gulf of Mexico coast (precip_06), and 3) a broader area of all of central and southwestern Mexico (precip_04). Both Mexico City and the Sierra Madre del Sur display a similar seasonal rainfall cycle (Figure DR7), which suggests that they are responding to the same broad-scale climate processes associated with the North American Monsoon. Further, rainfall amount in Mexico City is significantly correlated with onshore flow of Pacific Moisture, which must pass over the cave area prior to reaching Mexico City (Mosiño and Morales, 1988). The precipitation time series (Figure DR8) are compared to that at Tacubaya, and display a strong similarity at the multi-annual to decadal scales, suggesting that rainfall variations in Tacubaya are coherent with regional trends. Similar regional decadal scale rainfall variation was noted for Mexico City and other stations in the monsoon region of central and northern Mexico (Juaregui and Klaus, 1976). Additional evidence that climate processes are linked between the Sierra Madre del Sur and Mexico City is the strong correlation between JX-6 $\delta^{18}O$ and Mexico City rainfall amount. Given the 'noisy' nature of individual station precipitation data, we expect most of the shared variability to be at the multi-annual to decadal scale.

Additionally, analysis of rainfall data for southwestern and central Mexico shows that rainfall in the Basin of Mexico and the Sierra Madre del Sur are both strongly correlated to sea surface temperatures in the tropical Pacific Ocean (Liebmann et al., 2008). These data demonstrate that rainfall over the study area varies coherently with large-scale climate variability.

Cave and Stalagmite Description

We collected stalagmite JX-6 from deep within Juxtlahuaca Cave (Gay, 1967), near Colotlipa, Guerrero, in May of 2010. Juxtlahuaca Cave (17.4°N, 99.2ºW, 934 m a.s.l.) is located in the Sierra Madre del Sur, approximately 100 km northeast of Acapulco and 250 km south of Mexico City. Juxtlahuaca cave contains abundant predominantly aragonite stalagmites which are highly suitable for precise U-series dating. The cave also contains direct evidence of past Olmec ritual use from cave art and skeletal remains (Gay, 1967; Grove, 1969) and is located very near the epicenter of maize domestication in the Balsas River Valley (Piperno et al., 2009; Ranere et al., 2009). La Sorpresa is a dead-end passage that is stranded above the main Juxtlahuaca branch, and thus receives little to no air flow or visitation. We measured a relative humidity of 100% in the sampling room within Juxtlahuaca Cave on 4/29/2010 when the sample was collected, temperature of 24.8ºC, and 2875 ppm CO_2 concentration. On 6/5/11, relative humidity was 100% and temperature was 24.6ºC at the sample site, with a CO_2 concentration of 2293 ppm. No winds or circulation were evident in the sample passage of La Sorpresa on any visit to the cave over the past several years. Because of the high CO_2 concentration and very low drip rate, the stalagmite was likely inactive or accreting very slowly during the dry season. Our cave monitoring efforts (temperature, relative humidity, CO_2 concentration, drip activity) have just begun, so we do not have observations of drip activity to correlate to rainfall events.

Stalagmite JX-6 was collected in the La Sorpresa passage of Juxtlahuaca Cave (Figure DR9), at a distance of ~800 m from the entrance. Stalagmite JX-6 was collected from beneath an active drip, which had a very slow drip rate during the dry season collection date that did not allow for sampling. JX-6 was ~1 m tall in the cave, and its growth axis spans 1115 mm. The growth axis has shifted slightly over time, likely in response to a shift in drip impact site. A comparison of drip axis changes and stable isotope values indicates there is no relationship between the two. The stalagmite consists of white aragonite with porosity-defined banding. The base of the stalagmite has darker layers that are associated with hiatuses, and these were avoided in the current study. The base of the stalagmite dates to ca. 4000 yr BP, but slow and discontinuous growth prevailed until ca. 2400 year, after which time growth was rapid and uninterrupted by hiatuses.

High-precision laser and compass surveying in May of 2010 by Keith Christenson and Laura Rosales Lagarde produced a cave map that allowed estimation of thickness of bedrock over the JX-6 sample site of approximately 160 m. Such a thick epikarst is consistent with our inferred 9-yr lag between rainfall amount and $\delta^{18}O$ variations, and is consistent with diffuse flow. Nearby sections of the La Sorpresa passage show evidence for drip undersaturation, as evident from solutional 'drilling' in inactive stalagmite tips. This observation suggests relatively rapid communication with the ground surface, likely through conduit flow, which is short enough for drip waters to not achieve saturation with $CaCO_3$ during transit through the epikarst. In contrast, no such evidence for solutional drilling is evident near stalagmite JX-6, suggesting that this section of the passage is dominated by diffuse and not conduit flow. Observations by cave guides indicate a distinct seasonality of drip activity, reaching a high during the end of the wet season. That the cave drips have a seasonality, while our lag correlograms between $\delta^{18}O$ and rainfall amount indicate a 5-11 year lag, indicates that water is stored in the epikarst during the dry, slow-drip season.

Table 1. U-series data for stalagmite JX-6

Depth (mm)	^{238}U (ng/g)	^{232}Th (pg/g)	$^{230}Th/^{232}Th$ activity ratio	$^{230}Th/^{238}U$ activity ratio	Measured $\delta^{234}U$ (‰)	Initial $\delta^{234}U$ (‰)	Uncorrected age (yr BP)	Corrected age (yr BP)
3	17019 ± 46	35 ± 67	269 ± 522	0.000180 ± 0.000011	1049 ± 2	1049 ± 2	10 ± 1	**10 ± 1**
28	15897 ± 39	57 ± 71	869 ± 1091	0.001018 ± 0.000016	1062 ± 1	1062 ± 1	54 ± 1	**54 ± 1**
50	26451 ± 69	26 ± 56	5681 ± 12424	0.001814 ± 0.000012	1068 ± 1	1068 ± 1	96 ± 1	**96 ± 1**
75	7079 ± 19	7 ± 59	9715 ± 80330	0.003224 ± 0.000035	1069 ± 2	1070 ± 2	170 ± 2	**170 ± 2**
100	12066 ± 32	14 ± 77	13628 ± 76486	0.005093 ± 0.000035	1071 ± 1	1072 ± 1	269 ± 2	**269 ± 2**
125	4676 ± 13	26 ± 62	3662 ± 8798	0.006653 ± 0.000062	1074 ± 2	1075 ± 2	351 ± 3	**351 ± 3**
150	9796 ± 28	11 ± 63	22669 ± 134203	0.008000 ± 0.000044	1086 ± 1	1088 ± 1	419 ± 2	**419 ± 2**
200	4525 ± 12	7 ± 59	18656 ± 151901	0.009799 ± 0.000082	1070 ± 2	1073 ± 2	518 ± 4	**518 ± 4**
300	3305 ± 9	8 ± 73	17390 ± 165142	0.013317 ± 0.000112	1073 ± 2	1075 ± 2	704 ± 6	**704 ± 6**
400	6743 ± 17	12 ± 56	30056 ± 137290	0.017776 ± 0.000095	1037 ± 2	1039 ± 2	957 ± 5	**957 ± 5**
500	5425 ± 14	13 ± 37	28171 ± 81221	0.021786 ± 0.000098	1067 ± 2	1070 ± 2	1156 ± 5	**1156 ± 5**
600	5333 ± 14	11 ± 68	38949 ± 235968	0.026870 ± 0.000133	1054 ± 1	1058 ± 1	1436 ± 7	**1436 ± 7**
700	5950 ± 18	30 ± 42	17961 ± 24797	0.030092 ± 0.000130	1064 ± 1	1069 ± 1	1602 ± 7	**1602 ± 7**
800	7907 ± 25	41 ± 75	20061 ± 36649	0.034060 ± 0.000164	1023 ± 2	1029 ± 2	1851 ± 9	**1851 ± 9**
902	5114 ± 13	18 ± 59	34722 ± 112897	0.040382 ± 0.000170	1115 ± 3	1121 ± 3	2102 ± 9	**2102 ± 9**
981	5689 ± 16	54 ± 87	13919 ± 22250	0.043628 ± 0.000203	1134 ± 3	1141 ± 3	2252 ± 11	**2252 ± 11**
992	3490 ± 9	29 ± 61	17507 ± 36740	0.048025 ± 0.000222	1116 ± 3	1123 ± 3	2503 ± 12	**2503 ± 12**
1002	6415 ± 18	4 ± 67	299730 ± 5330877	0.057682 ± 0.000240	1050 ± 2	1060 ± 2	3109 ± 13	**3109 ± 13**
1035	9900 ± 27	52 ± 49	42269 ± 39898	0.072679 ± 0.000299	1047 ± 1	1059 ± 1	3936 ± 17	**3936 ± 13**
1041	1151 ± 3	124 ± 76	2137 ± 1310	0.075480 ± 0.000440	1049 ± 2	1062 ± 2	4085 ± 24	**4084 ± 24**

Corrected ages use an average crustal value for the initial $^{230}Th/^{232}Th$ atomic ratio = 4.4 ± 2.2 ppm. Years before present = yrs BP, where present is AD 2010. All errors are absolute 2σ. Subsample sizes range from 50 to 130 mg. $\delta^{234}U = ([^{234}U/^{238}U]_{activity} - 1) \times 1000$. $[^{230}Th/^{238}U]_{activity} = 1 - e^{-\lambda_{230}T} + (\delta^{234}U_{measured}/1000)[\lambda_{230}/(\lambda_{230} - \lambda_{234})](1 - e^{-(\lambda_{230} - \lambda_{234})T})$, where T is the age. Decay constants (λ) are 9.1577×10^{-6} year^{-1} for ^{230}Th, 2.8263×10^{-6} year^{-1} for 234U, and 1.55125×10^{-10} year^{-1} for ^{238}U.

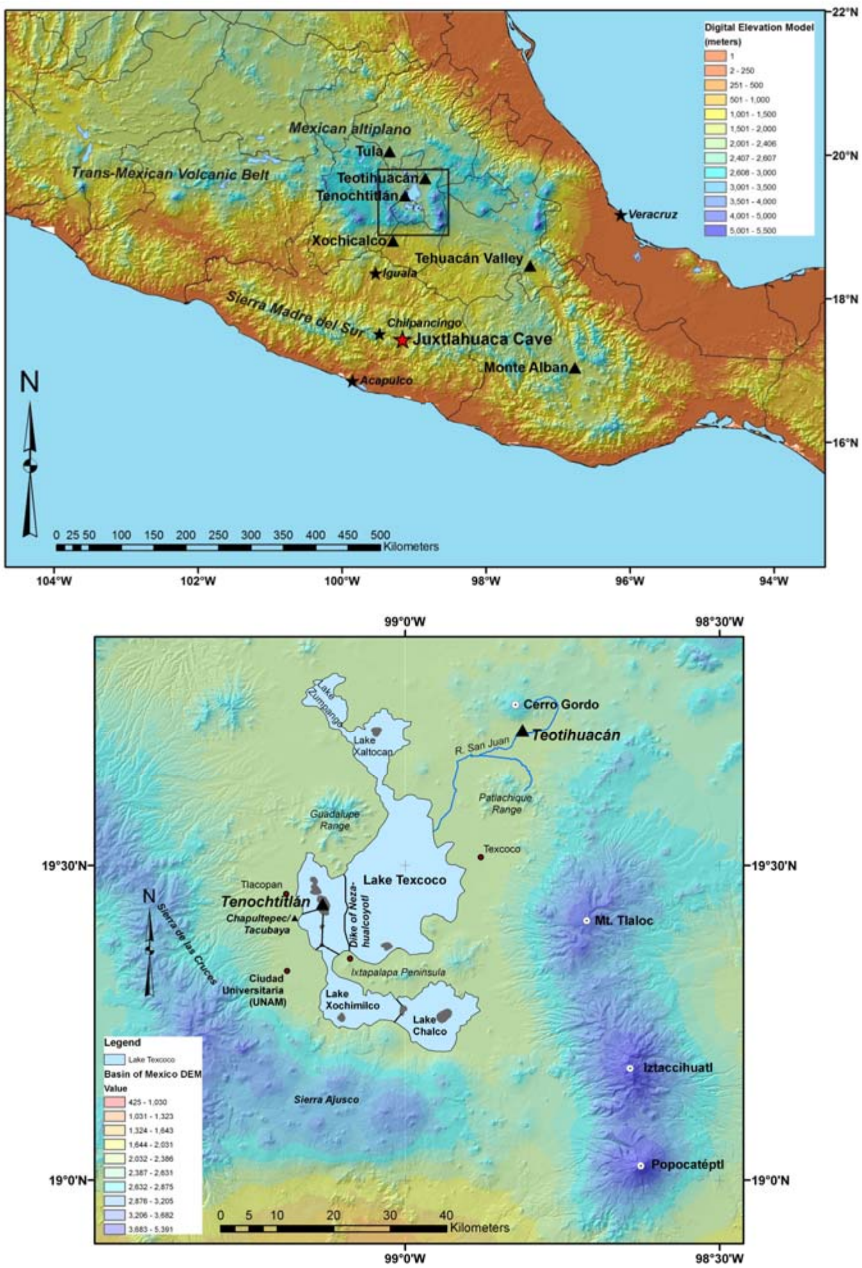

Figure DR1. Maps of the study area. Top is a digital elevation model draped of hillshade relief of southern Mexico, including physiographic features and prominent cultural sites. Rectangle shows detail at bottom. Bottom is a location map of the Basin of Mexico and the Teotihuacán sub-basin northeast of Lake Texcoco. Also shown are the sites mentioned in text, and basin lakes approximately at their extent ca. 1519 CE. Modern Mexico City is centered on the former island of Tenochtitlan and fills most of the area formerly occupied by western Lake Texcoco. Islands in grey and causeways and the dike of Nezahualcoyotl are shown in black lines. Colors are a digital elevation model in meters draped on a hill shade relief map.

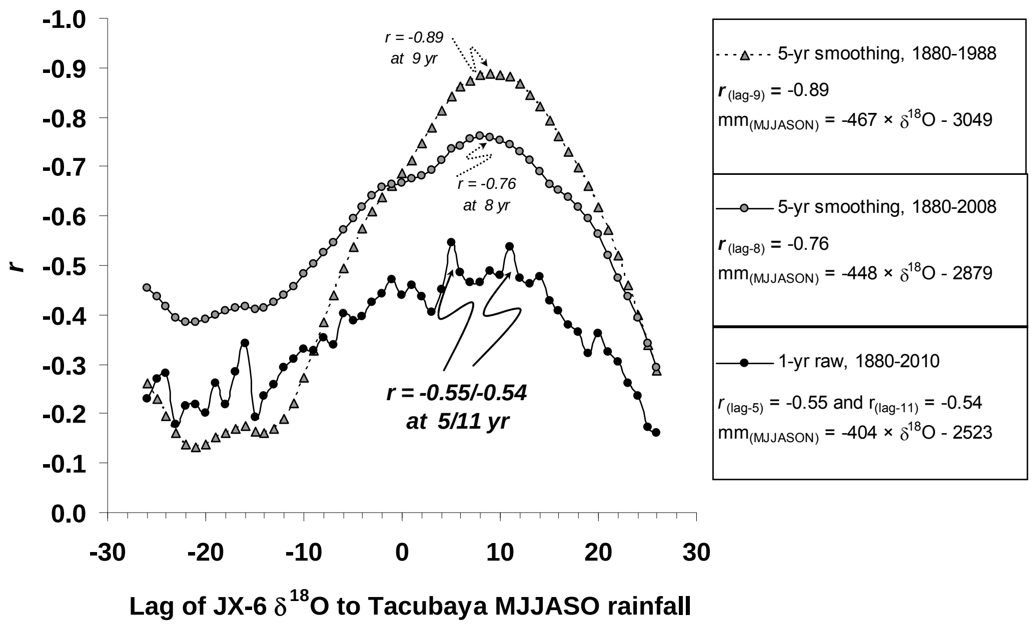

Figure DR2: Lag correlogram for the JX-6 $\delta^{18}O$/Tacubaya precipitation calibration. Bottom curve is the correlation between 1-yr interpolated $\delta^{18}O$ and Tacubaya MJJASON rainfall between 1880-2010 (black circles), with maximum correlations at 5 (*r* = -0.55) and 11 yr (*r* = -0.54). Grey circles are the correlogram for the 5-yr running averaged $\delta^{18}O$ and rainfall over 1880-2008, and grey diamonds for the 5-yr running averaged $\delta^{18}O$ and rainfall over 1880-1988, which excludes the Tacubaya rainfall data that may be compromised by anthropogenic effects. In the legend, calibration equations are given for the strongest lag for each statistical subset.

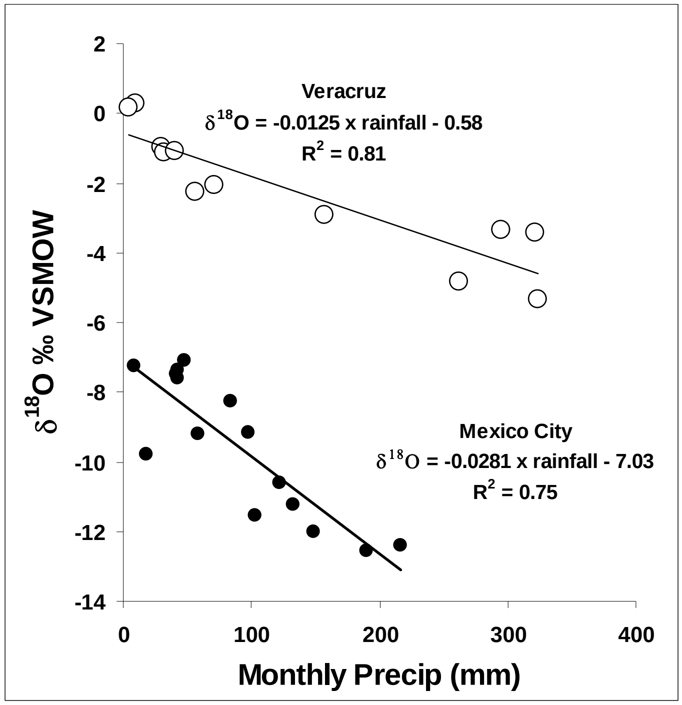

Figure DR3. Plot of rainfall $\delta^{18}O$ against monthly precipitation at Veracruz, and Mexico City (Ciudad Universitaria), Mexico. The open circles are Veracruz average monthly data (n=12 months), and filled circles are average monthly $\delta^{18}O$ values at Ciudad Universitaria (UNAM) for three wet seasons (June to October; n=18). The data from both Veracruz and Mexico City show a clear seasonal relationship with lower $\delta^{18}O$ values during the summer wet season that is driven by the amount effect.

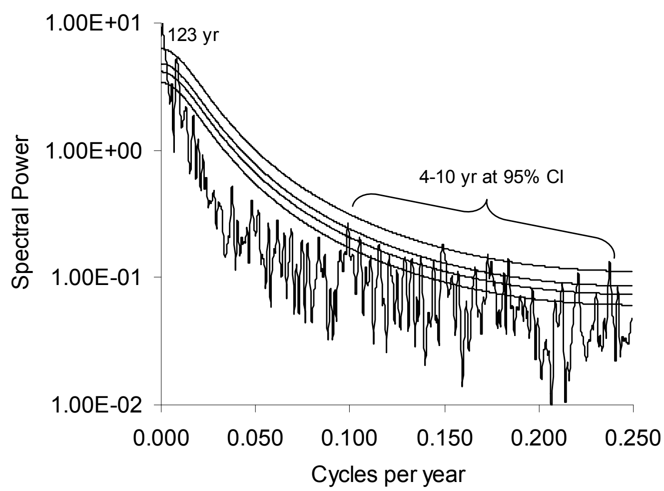

Figure DR4. Spectral analysis of the raw JX-6 $\delta^{18}O$ record. The 80, 90, 95, and 99% significance levels are shown (from bottom to top). Periods significant at above the 95% confidence intervals are shown with numerals. The data show spectral power in the near ENSO-band of 4-10 yr.

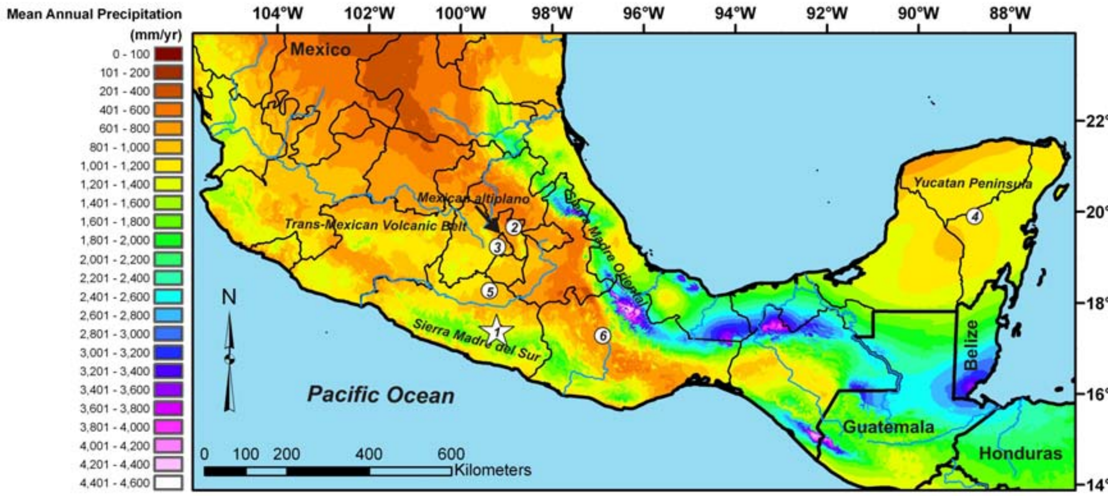

Figure DR5. Map of mean annual precipitation (in colors, mm/yr) of study area with sites mentioned in text. Star is location of Juxtlahuaca Cave, 2) Teotihuacán, 3) Tenochtitlán and Tacubaya climate station, 4) Lake Chichancanab, 5) lakes in Iguala Valley, 6) Monte Alban, Oaxaca.

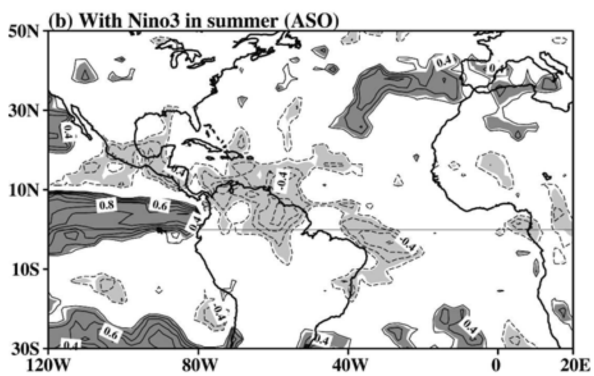

Figure DR6. Correlation of August through October precipitation anomalies with the Niño-3 SST index. Negative values (light grey shading enclosed with dashed contours) indicate dry conditions during warm El Niño events, throughout most of southern Mexico and Central America. From (Wang et al., 2006).

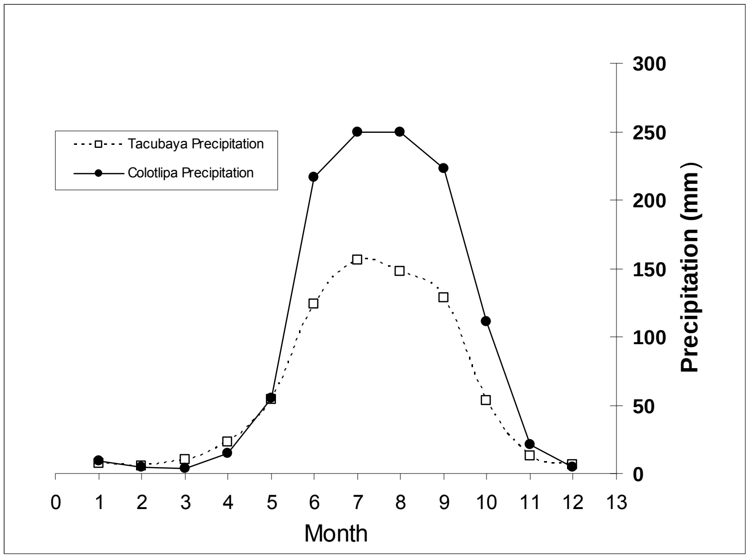

Figure DR7. Seasonal rainfall totals at Tacubaya (Mexico City) and Colotlipa (near Juxtlahuaca Cave) show similar seasonal cycles, but Tacubaya receives less rainfall.

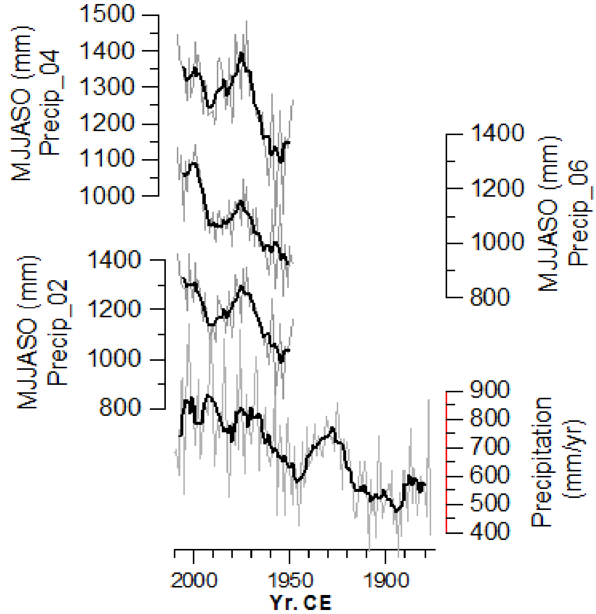

Figure DR8. Plot of NCEP wet season rainfall compared to the Tacubaya record shows strong similarities, particularly on the decadal scales.

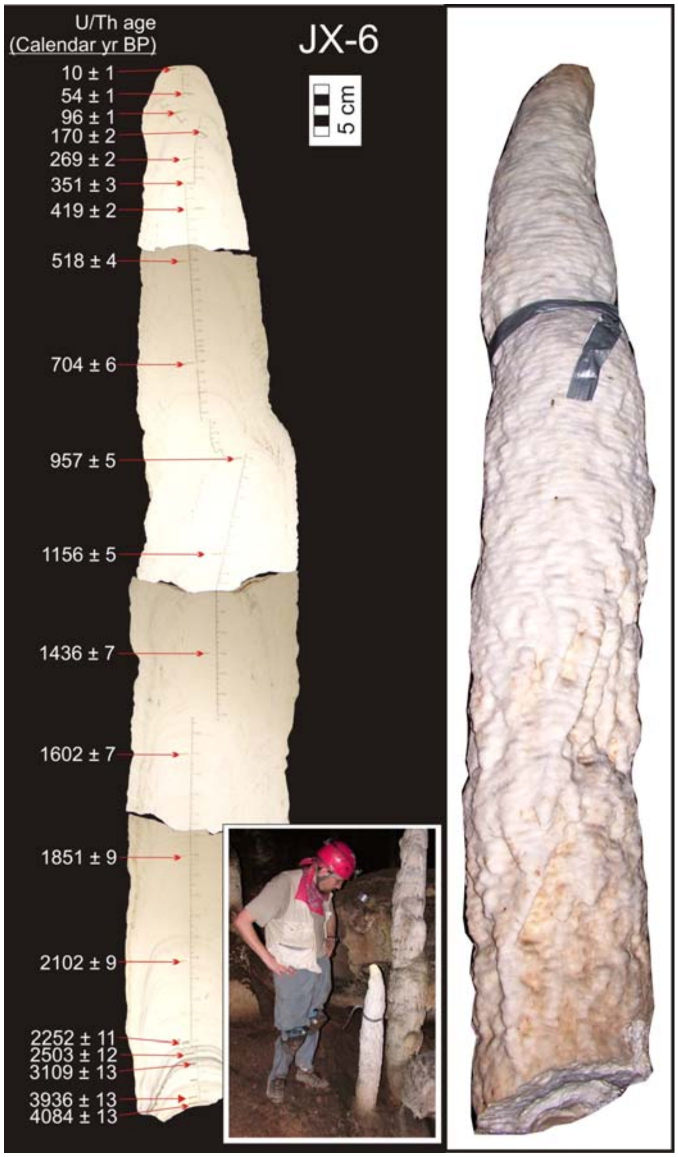

Figure DR9: Image of stalagmite JX-6. Inset shows JX-6 in growth position within the cave (with tape wrapped around the tip). Left shows the cut and polished slabs and the locations of the U-series ages, and the stable isotope sample transects, which were chosen to follow the central growth axis. Growth banding is very subtle and difficult to photograph because of the bright white color of the aragonite. Right is an image of the un-cut stalagmite to the same scale as the slabs.

References Cited

Adams, D. K., and Comrie, A. C., 1997, The North American Monsoon: Bulletin of the American Meteorological Society, v. 78, no. 10, p. 2197-2213.

Amador, J. A., Alfaro, E. J., Lizano, O. G., and Magaña, V. O., 2006, Atmospheric forcing of the eastern tropical Pacific: A review: Progress in Oceanography, v. 69, p. 101-142.

Asmerom, Y., Polyak, V., Schwieters, J., and Bouman, C., 2006, Routine high-precision U-Th isotope analyses for paleoclimate chronology: Geochimica et Cosmochimica Acta, v. 70, no. 18, Supplement 1, p. A24.

Barlow, M., Nigam, S., and Berbery, E. H., 1998, Evolution of the North American Monsoon system: Journal of Climate, v. 11, p. 2238-2257.

Cavazos, T., and Hastenrath, S., 1990, Convection And Rainfall Over Mexico And Their Modulation By The Southern Oscillation: International Journal Of Climatology, v. 10, no. 4, p. 377-386.

Chelton, D. B., Freilich, M. H., and Esbensen, S. K., 2000, Satellite observations of the wind jets off the Pacific coast of Central America. Part I: Case studies and statistical characteristics: Monthly Weather Review, v. 128, p. 1993-2018.

Cheng, H., Edwards, R. L., Hoff, J., Gallup, C. D., Richards, D. A., and Asmerom, Y., 2000, The half-lives of uranium-234 and thorium-230: Chemical Geology, v. 169, no. 1-2, p. 17-33.

Cortez-Vazquez, M., 1999, Annual cycle of convective activity in Mexico: Atmósfera, v. 12, no. 2, p. 101-110.

Curtis, S., 2004, Diurnal cycle of rainfall and surface winds and the mid-summer drought of Mexico/Central America: Climate Research, v. 27, p. 1-8.

Dai, A., and Wigley, T. M. L., 2000, Global patterns of ENSO-induced precipitation: Geophysical Research Letters, v. 27, no. 9, p. 1283-1286.

Douglas, M. W., Maddox, R. A., and Howard, K., 1993, The Mexican Monsoon: Journal of Climate, v. 6, p. 1665-1677.

Gay, C. T. E., 1967, Oldest Paintings of the New World: Natural History, v. 4, p. 28-35.

Grove, D. C., 1969, Olmec Cave Paintings - Discovery from Guerrero Mexico: Science, v. 164, no. 3878, p. 421-&.

Higgins, R. W., Chen, Y., and Douglas, A. V., 1999, Interannual variability of the North American warm season precipitation regime: Journal of Climate, v. 12, no. 3, p. 653-680.

Jauregui, E., 1995, Rainfall fluctuations and tropical storm activity in Mexico: Erdkunke, v. 49, p. 39-48.

Juaregui, E., 1990/1991, Influence of a large urban park on temperature and convective precipitation in a tropical city: Energy and Buildings, v. 15-16, p. 457-463.

Juaregui, E.,1992, Aspects of monitoring local/regional climate change in a tropical region: Atmósfera, v. 5, p. 69-78.

Juaregui, E., and Klaus, D., 1976, Some aspects of climate fluctuations in Mexico in relation to drought: Geofisica Internacional, v. 16, p. 45-61.

Kalnay, E., Kanamitsu, M., Kistler, R., Collins, W., Deaven, D., Gandin, L., Iredell, M., Saha, S., White, G., Woollen, J., Zhu, Y., Chelliah, M., Ebisuzaki, W., Higgins, W., Janowiak, J., Mo, K. C., Ropelewski, C., Wang, J., Leetmaa, A., Reynolds, R., Jenne, R., and Joseph, D., 1996, The NCEP/NCAR 40-year reanalysis project: Bulletin of the American Meteorological Society, v. 77, no. 3, p. 437-471.

Lauer, W., 1973, The altitudinal belts of the vegetation in the central Mexican highlands and their climatic conditions: Arctic and Alpine Research, v. 5, no. 3, p. A99-A113.

Liebmann, B., Blade, I., Bond, N. A., Gochis, D., Allured, D., and Bates, G. T., 2008, characteristics of North American monsoon summertime rainfall with emphasis on the Monsoon: Journal of Climate, v. 21, p. 1277-1294.

Magaña, R. V., 2004, Los impactos de El Niño en México, Centro de Ciencias de la Atmósfera, Universidad Nacional Autónoma de México, Secretaría de Gobernación. México,, p. 229.

Magaña, V. O., Vazquéz, J. L., Pérez, J. L., and Pérez, J. B., 2003, Impact of El Niño on precipitation in Mexico: Geofísica Internacional, v. 42, no. 3, p. 313-330.

Mendoza, B., Jauregui, E., Diaz-Sandoval, R., Garcia-Acosta, V., Velasco, V., and Cordero, G., 2005, Historical droughts in central Mexico and their relation with El Niño: Journal of Applied Meteorology, v. 44, no. 5, p. 709-716.

Mosiño-Alemán, P. A., and García, E., 1974, The climate of Mexico, *in* Bryson, R. A., and Hare, F. K., eds., Climates of North America: New York, Elsevier, p. 345-404.
Mosiño, P. A., and Morales, T., 1988, Los ciclones tropicales, El Niño y las lluvias en Tacubaya, D.F.: Geofisica Internacional, v. 27, no. 1, p. 61-82.
Piperno, D. R., Ranere, A. J., Holst, I., Iriarte, J., and Dickau, R., 2009, Starch grain and phytolith evidence for early ninth millennium B.P. maize from the Central Balsas River valley, Mexico: Proceedings of the National Academy of Sciences of the United States of America, v. 106, no. 13, p. 5019-5024.
Ranere, A. J., Piperno, D. R., Holst, I., Dickau, R., and Iriarte, J., 2009, The cultural and chronological context of early Holocene maize and squash domestication in the Central Balsas River Valley, Mexico: Proceedings of the National Academy of Sciences of the United States of America, v. 106, no. 13, p. 5014-5018.
Rogers, J. C., 1988, Precipitation variability over the Caribbean and tropical Americas associated with the Southern Oscillation: Journal of Climate, v. 1, p. 172-182.
Sáenz-Romero, C., Rehfeldt, G., Crookston, N., Duval, P., St-Amant, R., Beaulieu, J., and Richardson, B., 2010, Spline models of contemporary, 2030, 2060 and 2090 climates for Mexico and their use in understanding climate-change impacts on the vegetation: Climatic Change, v. 102, no. 3, p. 595-623.
Schmitz, J. T., and Mullen, S. L., 1996, Water vapor transport associated with the summertime North American Monsoon as depicted by ECMWF analyses: Journal of Climate, v. 9, p. 1621.
Schultz, D. M., Bracken, W. E., Bosart, L. F., Hakim, G. J., Bedrick, M. A., Dickinson, M. J., and Tyle, K. R., 1997, The 1993 superstorm cold surge: frontal structure, gap flow, and tropical impact: Monthly Weather Review, v. 125, no. 5-39.
Schulz, M., and Mudelsee, M., 2002, REDFIT; estimating red-noise spectra directly from unevenly spaced paleoclimatic time series: Computers & Geosciences, v. 28, no. 3, p. 421-426.
Servicio_Meteorológico_Nacional, 2008, http://smn.cna.gob.mx/.
Stahle, D. W., Cook, E. W., Villanueva, J., Diaz, F. K., Fye, D. J., Burnette, D. J., Griffin, R. D., Acuna-Soto, R., Seager, R., and R.R., H. J., 2009, Early 21st-century drought in Mexico: Eos, v. 90, no. 11, p. 89-100.
Stensrud, D. J., Gall, R. L., Mullen, S. L., and Howard, K. W., 1995, Model climatology of the Mexican Monsoon: Journal of Climate, v. 8, p. 1775-1794.
Wang, C., and Fiedler, P. C., 2006, ENSO variability and the eastern tropical Paific: A review: Progress in Oceanography, v. 69, p. 239-266.
Wang, C. Z., Enfield, D. B., Lee, S. K., and Landsea, C. W., 2006, Influences of the Atlantic warm pool on western hemisphere summer rainfall and Atlantic hurricanes: Journal of Climate, v. 19, no. 12, p. 3011-3028.